ARTICLES

The structural basis of calcium transport by the calcium pump

Claus Olesen[1,2], Martin Picard[3]†, Anne-Marie Lund Winther[1,3], Claus Gyrup[3], J. Preben Morth[1,3], Claus Oxvig[3], Jesper Vuust Møller[1,2] & Poul Nissen[1,3]

The sarcoplasmic reticulum Ca^{2+}-ATPase, a P-type ATPase, has a critical role in muscle function and metabolism. Here we present functional studies and three new crystal structures of the rabbit skeletal muscle Ca^{2+}-ATPase, representing the phosphoenzyme intermediates associated with Ca^{2+} binding, Ca^{2+} translocation and dephosphorylation, that are based on complexes with a functional ATP analogue, beryllium fluoride and aluminium fluoride, respectively. The structures complete the cycle of nucleotide binding and cation transport of Ca^{2+}-ATPase. Phosphorylation of the enzyme triggers the onset of a conformational change that leads to the opening of a luminal exit pathway defined by the transmembrane segments M1 through M6, which represent the canonical membrane domain of P-type pumps. Ca^{2+} release is promoted by translocation of the M4 helix, exposing Glu 309, Glu 771 and Asn 796 to the lumen. The mechanism explains how P-type ATPases are able to form the steep electrochemical gradients required for key functions in eukaryotic cells.

P-type cation pumps constitute an important family among actively transporting ATPases, with fundamental roles in cell function and in maintaining the cellular environment. Prominent examples include Ca^{2+}-ATPases and Na^+,K^+-ATPase, which alone consume approximately one-third of the energy used in humans[1]. Besides cation pumps, P-type ATPases are of critical importance in the homeostasis of heavy metals and the asymmetric distributions of lipids in membranes. The transport processes of the P-type ATPases are based on cyclical changes between two main conformational states, denoted E1 and E2, during which the ATPase is phosphorylated by ATP at a conserved aspartic acid side chain, and subsequently dephosphorylated. These processes are coupled to vectorial transport and counter transport by the controlled opening and closing of cytoplasmic and extracellular/luminal pathways.

Ca^{2+}-ATPases energize the Ca^{2+}-mediated signalling networks of the cell and maintain steep Ca^{2+} gradients across plasma membranes and inner membranes[2]. The sarco-endoplasmic reticulum Ca^{2+}-ATPase isoform 1a (SERCA1a) pumps Ca^{2+} from the cytosol of skeletal muscle cells into the sarcoplasmic reticulum store, thereby terminating a muscle contraction event[3]. SERCA1a activity results in transmembrane Ca^{2+} concentration ratios of three to four orders of magnitude (from a sub-micromolar to a millimolar level), in a high coupling ratio (approaching 2:1) of Ca^{2+} transport with ATP hydrolysis[4,5], and with counter transport of luminal protons[6–8].

Several aspects of the structure and overall transport mechanism of rabbit SERCA1a are well understood as a result of numerous investigations into the functional properties and owing to a range of crystal structures representing well-defined states of the functional cycle[9–15]. SERCA1a is composed of ten transmembrane helices (M1 through M10) and three cytosolic domains[9]: N (nucleotide binding), P (phosphorylation) and A (actuator). In its E1 form, SERCA1a binds two Ca^{2+} ions with high affinity in the middle of the ten transmembrane helices, whereas in the E2 form the cation-binding sites are associated with protons. Of particular importance, it has been shown that transition states of phosphorylation and dephosphorylation (as studied by aluminium fluoride complexes) are coupled to occlusion of bound calcium[11,12] and protons[14], respectively. In the forward direction of the functional cycle, the $Ca_2E1{\sim}P$ state, formed by reaction of Ca_2E1 with ATP, is converted to an E2P state, accompanied by translocation of Ca^{2+}. The E2P state is then dephosphorylated along with a counter transport of protons. All steps in the reaction cycle are reversible; thus ADP stimulates the dephosphorylation of the $Ca_2E1{\sim}P$ state through regeneration of ATP, and Ca^{2+}/Ca^{2+} exchange is observed at high vesicular levels of Ca^{2+} (refs 16–18) .

Despite detailed insight into the occluded transition states of phosphorylation and dephosphorylation, structural information on the essential step by which Ca^{2+} is transferred from the cytosol into the intraluminal space of sarcoplasmic reticulum vesicles is lacking. Does it occur through a gated channel (as, for example, suggested for Na^+,K^+-ATPase[19]) or is it the result of conformational changes that project the intramembrane binding sites towards the vesicle lumen[20]? In this article we address this question on the basis of new crystal structures of the Ca^{2+}-ATPase, all obtained in the absence of inhibitors bound in the membrane, namely: (1) the $Ca_2E1{\sim}P$ state formed by adenosine 5′-(β,γ-imido)-triphosphate (AMPPNP) and determined at 2.8 Å resolution, (2) an E2-BeF_3^- complex, representing a genuine E2P state, determined at 2.65 Å resolution, and (3) a structure determined at 3.0 Å resolution of the E2-AlF_4^- complex in the presence of the non-hydrolysable ATP analogue adenosine 5′-(β,γ-methylene)-triphosphate (AMPPCP), representing the ATP-modulated transition state of dephosphorylation, here denoted as E2-P*. We show how product separation in the high-energy $Ca_2E1{\sim}P$ state allows for the transition to the E2P state with exposure of a luminal pathway, which is resealed on the subsequent replacement of Ca^{2+} by H^+ and through formation of a dephosphorylation site in the E2-P* state. Together, these studies complete the overall view of SERCA1a structure and function and provide rationales that can be transferred to all members of the P-type ATPase family.

[1]Centre for Membrane Pumps in Cells and Disease—PUMPKIN, Danish National Research Foundation, and [2]Institute of Physiology and Biophysics, University of Aarhus, Ole Worms Alle, blg. 1185, DK - 8000 Aarhus C, Denmark. [3]Department of Molecular Biology, University of Aarhus, Gustav Wieds Vej 10C, DK - 8000 Aarhus C, Denmark. †Present address: Laboratoire de Cristallographie et RMN biologiques, UMR 8015 CNRS, Faculté de Pharmacie. Université Paris Descartes, 4 avenue de l'Observatoire, 75270 Paris Cedex 06, France.

Overall comparison of new structures

Crystals were obtained in the presence of native lipids and crystal structures were determined as described in Methods.

The three structures are shown in Fig. 1, along with the previously published structure of the ATP-bound E2 state[15] (using AMPPCP). Together, these structures represent a minimal scheme comprising four cornerstones of the functional cycle. Conformational changes occur as a result of concerted movements of transmembrane helices connecting the reactions at the phosphorylation site with binding events at the cation-binding sites in the membrane. The coupling is transmitted through movements of the A domain. Worth noting, E2-BeF_3^-– and E2-AlF_4^-–AMPPCP complexes are the first structures obtained of calcium-free SERCA1a without structural bias from membrane domain inhibitors like thapsigargin[10,14,15,21,22].

The Ca_2E1~P state

The conformation of SERCA1a crystallized in the presence of Ca^{2+} and AMPPNP is similar to the Ca_2E1-AMPPCP and Ca_2E1-ADP-AlF_4^- forms described earlier as the pre-state and transition state of phosphorylation, respectively, associated with occlusion of two Ca^{2+} ions in the membrane[11,12]. However, unbiased difference Fourier maps show important changes at the phosphorylation site (Fig. 2a), indicating that a genuine aspartyl-phosphoanhydride has formed at Asp 351 along with AMPPN (like ADP) at the nucleotide-binding pocket. The changes result in a ~3.1 Å net separation of the (bridging) β,γ-imido nitrogen and the γ-phosphoryl group transferred to Asp 351. The authenticity of phosphoenzyme formation was confirmed by mass spectrometry of re-dissolved crystals (Supplementary Fig. 1). In experiments on sarcoplasmic reticulum vesicles we also confirmed a previous finding[23] that SERCA1a cleaves AMPPNP in a Ca^{2+}-dependent reaction. The hydrolysis rate of AMPPNP (with a V_{max} of around 1 nmol per mg of protein per min at pH 7.1 and 23 °C) is approximately 5,000 times slower than observed with saturating amounts of ATP, yet Ca^{2+} transport is sustained with a high coupling ratio of 1.5 (±0.2):1 (Fig. 2b, c, and Supplementary Fig. 2), corresponding to what is observed with ATP at similar conditions[17,24]. In other words, AMPPNP is a fully functional but slow substrate for SERCA. The AMPPN (ADP) remains enclosed at the phosphorylation site with the aspartyl-phosphoanhydride trapped in a high-energy product complex, in accordance with the Ca_2E1~P state being ADP sensitive.

An important consequence of phosphorylation is that the nucleotide no longer bridges across the interface between the N and P domains: the N domain with the ADP-leaving group can therefore separate from the P domain, whereas the aspartyl-phosphoanhydride interacts with residues and a divalent cation of the P domain (Fig. 2a). Unlocking the domain interface by phosphorylation allows the ATPase to explore other conformational states that, according to recent kinetic evidence, lead to the rapid and reversible formation of E2P[25], as established previously in connection with the Na^+-dependent phosphorylation of Na^+,K^+-ATPase[26,27].

The E2P state with an exit pathway exposed to the lumen

The E2-BeF_3^- structure reveals a new and unique conformation of SERCA1a, showing an open, luminal pathway (Fig. 1, and Supplementary Fig. 4). The Asp 351 side chain is covalently modified by BeF_3^- and associated with a Mg^{2+} ion (Fig. 3a), and the site is isosteric to that of the phosphorylated Ca_2E1~P state. We find that

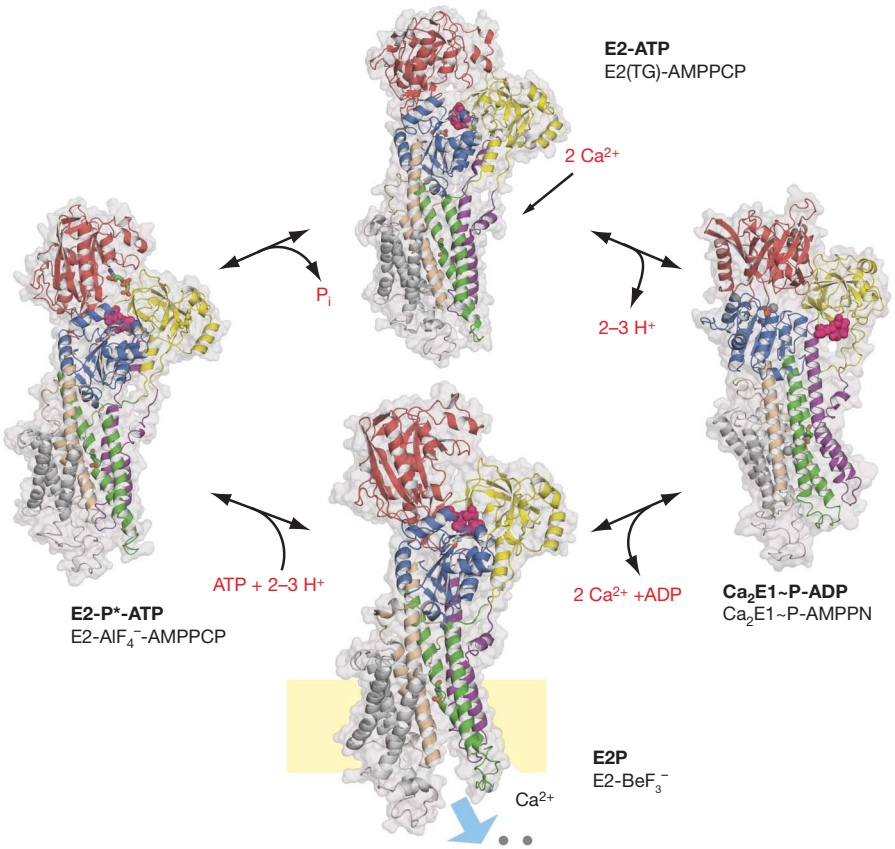

Figure 1 | Overall comparison of SERCA1a structures representing key states of the reaction cycle. The new structures of Ca_2E1~P-AMPPN, E2-BeF_3^- and E2-AlF_4^- complexes form the basis of this report and the E2-BeF_3^- complex is increased in size to emphasize its critical importance. Cation- and nucleotide-exchange reactions are indicated. The structures are depicted by grey, transparent surfaces and by cartoon representations, with the A domain in yellow, N domain in red, P domain in blue, transmembrane segment M1–2 in purple, M3–4 in green, M5–6 in wheat and M7–10 in grey. The TGES motif is shown by pink space-filling, residues 309, 771 and 796 (mentioned in the text) as sticks, and bound Ca^{2+} ions as grey spheres. Here, and in the following figures, structural representations were prepared with Pymol (http://pymol.sourceforge.net/).

BeF_3^- reacts with Ca^{2+}-ATPase with an affinity in the nanomolar range, yet our data also show that millimolar levels of Ca^{2+}, when granted access at the luminal side, lead to rapid and full re-activation of the BeF_3^--complexed Ca^{2+}-ATPase (Fig. 3b, c, and Supplementary Fig. 3), characteristic of an E2P state exposed to the lumen. Indeed, the signature by tryptophan fluorescence spectroscopy and a reduced Ca^{2+}-binding affinity have previously been used to argue that the BeF_3^--bound complex mimics the genuine E2P state[28,29].

A key question is then how phosphorylation has triggered the formation of an exit pathway? The answer is to be found in specific interactions of the A domain with the phosporylation site. The conserved TGES loop of the A domain replaces ADP and the N domain and forms a tight seal at the phosphorylation site by an extensive range of interactions with the Mg^{2+}-bound aspartyl phosphoanhydride (Fig. 3a, and see later). To yield this interaction of the TGES motif the A domain has rotated approximately 120° around the P domain and wedged itself into the N domain, which is now displaced from its interaction with the P domain. As a result of this movement the A domain exerts a powerful drag on transmembrane segments M1–M2 and M3–M4 and forces them to spread out and separate from M5–M6, which remain joined with the remaining transmembrane helices in an M5–M10 complex (Fig. 4). Indeed, intact linkers between the A domain and the membrane are of critical importance for Ca^{2+} transduction: thus proteolytic cleavage of the

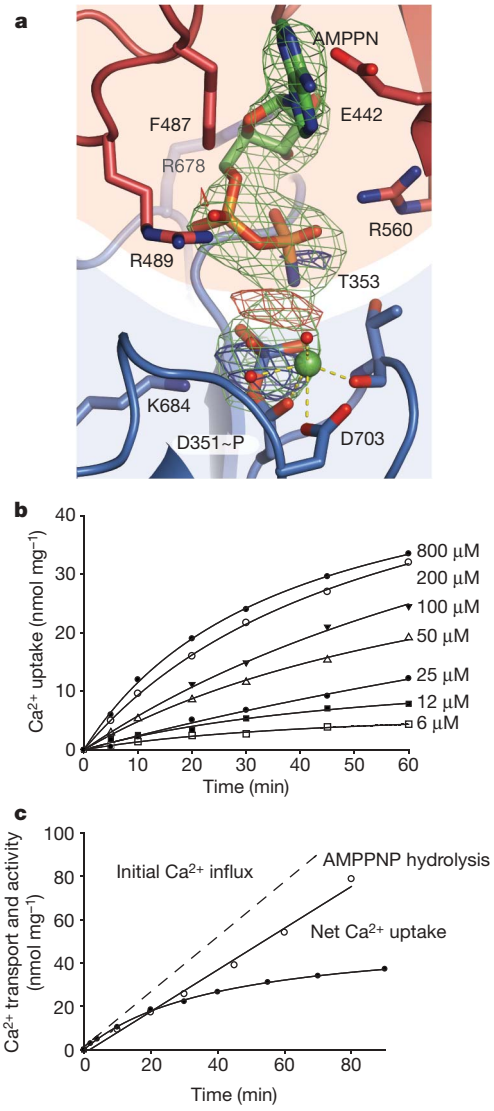

Figure 2 | The Ca2E1~P state obtained with AMPPNP. **a**, Refined structure (stick representation) of the Ca_2E1~P-AMPPN complex. The unbiased (F_O-F_C) difference map of the nucleotide complex (green mesh, 5.5σ), and the experimental ($F_O^{AMPPNP}-F_O^{ADP\text{-}AlF}$) difference map (−4σ and 4σ, red-brown and blue, respectively) show phosphoryl transfer to Asp 351. **b**, The upper panel shows Ca^{2+} accumulation by sarcoplasmic reticulum vesicles as a function of AMPPNP concentration. **c**, Ca^{2+} uptake, relative to AMPPNP hydrolysis at 200 μM of nucleotide. Dashed lines indicate initial rates of Ca^{2+} uptake, used for calculation of the coupling ratio (see text). The AMPPNP hydrolysis rate remains constant, whereas the Ca^{2+} transport rate declines owing to Ca^{2+}/Ca^{2+} exchange (J.V.M., unpublished observations).

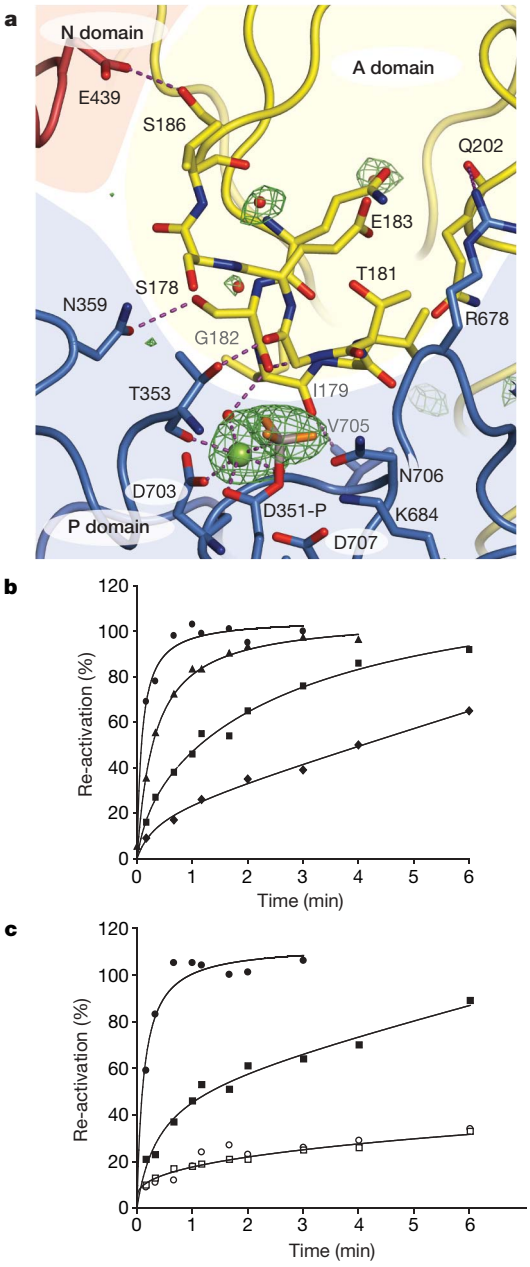

Figure 3 | The E2P state obtained with beryllium fluoride. **a**, Refined structure (stick representation) of the E2-BeF_3^- complex with unbiased (F_O-F_C) electron density shown at the phosphorylation site (5σ), showing BeF_3^- associated with Asp 351. Water molecules are shown as red spheres. **b**, **c**, Ca^{2+}-mediated displacement of BeF_3^- as a function Ca^{2+} concentration (circles, 10 mM; triangles, 5 mM; squares, 2 mM ; diamonds, 1 mM) using purified and leaky Ca^{2+}-ATPase preparations (**b**) or intact sarcoplasmic reticulum vesicles (**c**) in the presence (filled symbols) or absence (open symbols) of A23187 ionophore, thus distinguishing intravesicular and extravesicular effects of Ca^{2+}. *y* axis, recovery of activity relative to that of a BeF_3^- unmodified control; *x* axis, duration of Ca^{2+}-ATPase or vesicle exposure to 10 mM Ca^{2+}.

A-M3 linker[30] and shortening of the A-M1 linker[31] block formation of the E2P state, whereas proteolytic cleavage of the A-M2 linker[32] or extending the A-M1 linker[33] inhibit subsequent dephosphorylation of E2P, despite the conformational changes at the cytoplasmic domains. The transition of E1P—with a 10–15 Å hydrophobic barrier of the Ca^{2+}-binding sites to the lumen—to the E2P state leads to the formation of a three-lobed structure with a luminal pathway opening from the cation-binding sites towards the lumen (Fig. 4). The new configuration also distorts the calcium-binding sites in the membrane, primarily because of: (1) rotational movements of M6 bringing Asp 800 and Asn 796 away from their binding positions between Ca^{2+} sites I and II, (2) a ~6 Å translational movement of M4 with Glu 309 in the luminal direction, and (3) smaller translational movements of Glu 771 and Glu 908 (Fig. 4a, b). As a result, the luminal pathway exposes three of the Ca^{2+}-liganding residues, Glu 309 (site II), Glu 771 (site I) and Asn 796 (site I and II), to the lumen through a funnel-shaped polar pathway characterized by a width spanning from around 4 Å at the location of the exposed Ca^{2+}-liganding residues to around 15 Å at the luminal mouth of the pathway (Fig. 4d). In previous studies, exactly the same residues were pinpointed by site-directed mutagenesis as candidates for the luminal proton exchange during the reaction cycle[34,35]. The homologous residues in the occluded $K_2E2{\cdot}P_i$ state of Na^+,K^+-ATPase[36] (E327, E779, D804) interact with K^+ and are also important residues in formation of the E2P-like conformation of the palytoxin open channel[37].

The occluded E2-P* transition state without thapsigargin

The continuation of the functional cycle leads to the dephosphorylation reaction, as described earlier for the thapsigargin-bound complexes of SERCA1a with AlF_4^- mimicking the E2-P* transition state[14], or with MgF_4^{2-} mimicking the liberated but still entrapped phosphate of the $E2{\cdot}P_i$ state[13]. The authenticity of earlier E2 structures has been questioned, owing to the presence of thapsigargin or other inhibitors. However, the crystal structure of the E2-AlF_4^--AMPPCP complex obtained here in the absence of thapsigargin shows that the effect of the inhibitor is minimal (Supplementary Fig. 5), even at the binding pocket for thapsigargin between M3, M5 and M7. The inhibitory effect of thapsigargin thus seems to be based on trapping SERCA1a in the occluded E2 conformation. We have previously shown that the E2-AlF_4^- form represents an occluded state associated with the binding of probably 2–3 protons for counter transport[14], more correctly denoted H_{2-3}E2-AlF_4^-. Thus, during dephosphorylation, the M1–M2 and M3–M4 segments close against the M5–M10 region, burying the cation-binding residues in the membrane (Figs 1 and 4c). Worth noting, these residues adopt nearly the same configuration in thapsigargin (TG)-bound forms[10,13], and also in the E2-BeF_3^- complex, though stabilized by a Mg^{2+} ion in the latter (Fig. 4b, e). The reclosure of the transmembrane domain transmits to a ~10° perpendicular rotation of the A domain around the phosphorylation site of the P domain (away from the N domain and towards the membrane), in relation to which the TGES loop is moved by formation of a phosphorolytic site centred on Glu 183 (Fig. 5). The AMPPCP nucleotide of the E2-AlF_4^- complex (representing modulatory ATP) is bound at an exposed site centred on the Phe 487 region of the N domain and interacting with Lys 205 of the A domain (Fig. 5c), in a similar way to the binding of ADP to the E2(TG)-MgF_4^{2-} complex[13].

A nucleotide exchange mechanism of Ca^{2+}-ATPase

In transition from the Ca_2E1~P-ADP state to the E2P state the nucleotide-binding pocket at the N domain has gained access to the cytoplasmic environment, lined by the Arg 174 residue of the A domain (Fig. 5b). The E2-BeF_3^- structure (representing E2P) was obtained in the absence of nucleotide. However, AMPPN (representing the ADP leaving group) of the Ca_2E1~P-AMPPN nucleotide complex provides a snug fit in the E2-BeF_3^- structure when docked on the basis of a structural alignment of the N domain (Fig. 5b), and even when modelled as ATP. We suggest that this site provides the basis for ADP release in exchange for ATP in the E2P state. Putting this model into context with the structures of E2-AlF_4^--AMPPCP (this study), E2(TG)-AMPPCP[15], and the Ca_2E1~P-AMPPN form (this study) a systematic progression is observed during which ATP enters from an exchange site, moving to modulatory sites and then to

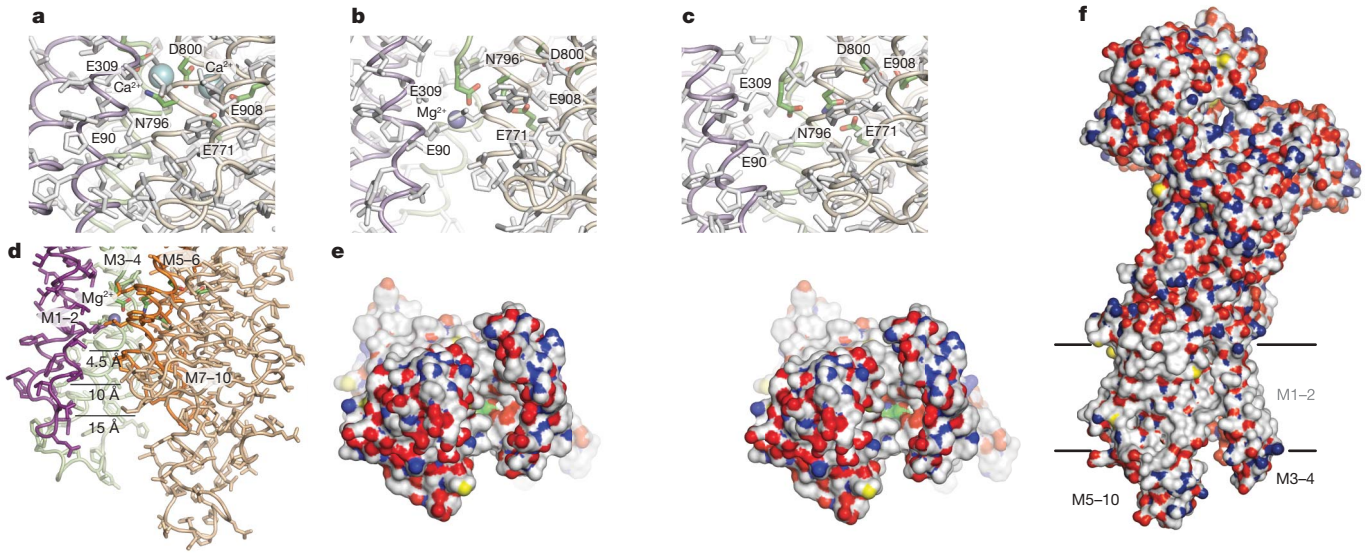

Figure 4 | The luminal exit pathway of sarcoplasmic reticulum Ca^{2+}-ATPase. **a**, The Ca_2E1~P form of SERCA1a (full stick representation and backbone trace) showing the Ca^{2+}-binding residues (carbon, green; oxygen, red; nitrogen, blue) and occluded Ca^{2+} ions (grey spheres). **b**, Same representation of the E2-BeF_3^- complex (grey-blue sphere for Mg^{2+}) with a similar orientation of the M7–10 region to **a**, now showing a luminal exit pathway and exposure of Ca^{2+} ligating residues. **c**, Similar representation of the E2-AlF_4^- structure with reclosure of the protonated state. **d**, Larger view of the E2-BeF_3^- form (as in **b**) with colours of transmembrane segments as in Fig. 1. Approximate dimensions of the funnel-shaped exit pathway are indicated. **e**, Stereoview of the E2-BeF_3^- complex (space-filling) as seen from the luminal side onto the membrane and showing a polar surface of the exit pathway. Carbon, white; sulphur, yellow; nitrogen, blue; oxygen, red, except for Ca^{2+}-binding residues, green (Glu 309, Glu 771 and Asn 796). **f**, Sideview of the E2-BeF_3^- complex (perpendicular to **e**), displaying well-defined boundaries of an apolar surface for membrane localization.

the final catalytic site as the enzyme proceeds from E2P (Fig. 5b) in the forward direction by Ca^{2+}-activated phosphorylation (Fig. 5). The Arg 174 residue of the A domain would seem to stabilize nucleotide binding in the E2P state. This residue is not conserved among P-type ATPases and may be the basis of the SERCA-specific ATP modulation of the $Ca_2E1{\sim}P$ to E2P transition[38].

Discussion

The present data indicate how two cytoplasmic Ca^{2+} ions, occluded in the membrane in the $Ca_2E1{\sim}P$ state, can be transferred to the lumen of the sarcoplasmic reticulum vesicles via an open luminal pathway formed by the separation of the M1–M2, M3–M4 and the M5–M6 segments in the E2P state. The transition also results in a decrease in Ca^{2+}-binding affinity owing to a change in the configuration of the liganding residues so that Ca^{2+} can be efficiently translocated from a low- to a high-concentration environment. The energy required is ultimately derived from ATP hydrolysis at the phosphorylation site—the motor of the pump—via a phosphoenzyme intermediate. All steps of the cycle are reversible, so how is efficient transport maintained as the electrochemical gradient builds up? The answer is to be found in the structural characteristics of the pump with the A domain linked to segments M1 through M3 to control the opening and closing of the luminal pathway, and the energetic input from the P domain connected to the membrane by the cytoplasmic extensions of M4 and M5. This provides the basis for coupling between the cation-binding sites in the membrane and the chemical processes occurring at the phosphorylation site. Furthermore, the physiological working conditions with a high ATP-to-ADP ratio in the cell have an important modulatory role, keeping the protein in a compact, nucleotide-bound state during the whole cycle (Figs 1 and 5).

To summarize, starting from the ATP-bound $H_{2-3}E2$ state (Figs 1 and 6), release of protons from the cation-liganding residue, in exchange for cytoplasmic Ca^{2+} ions, leads to the assembly of the phosphorylation site with the ATP-bound N domain[15], and with the A domain directing the occlusion of bound Ca^{2+} (refs 11 and 12). The $Ca_2E1{\sim}P$ state is formed through a favourable kinase activity producing ADP and an energy-rich aspartyl-phosphoanhydride bond, which unleashes the N domain from the P domain as the

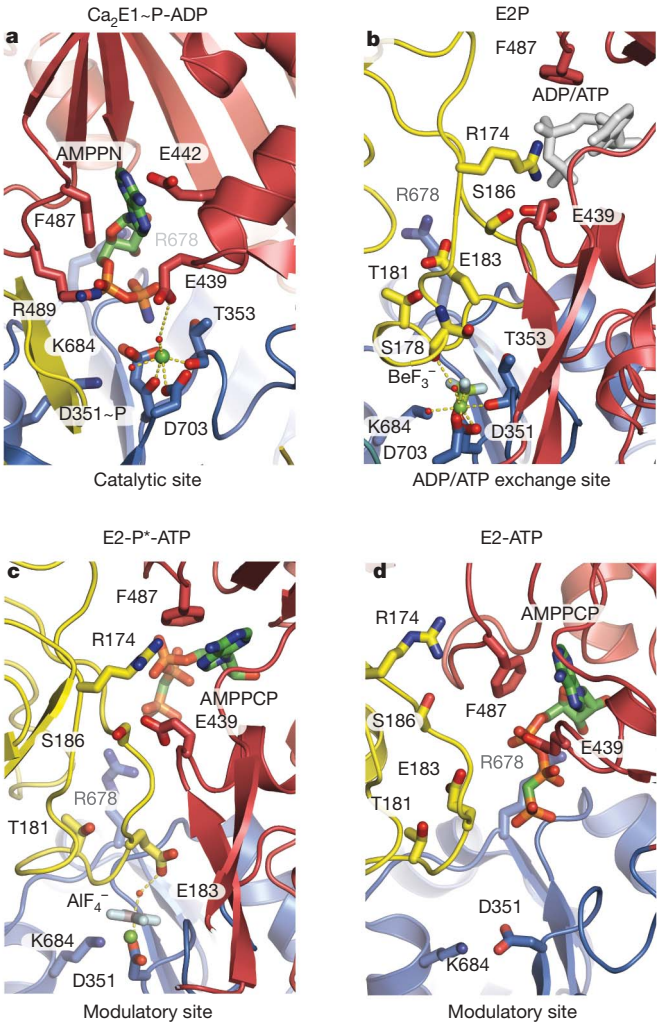

Figure 5 | Changes at the phosphorylation site of SERCA1a in the functional cycle. Structures are shown as a cartoon with selected residues in stick representation and with domain colours as in Fig. 1. The functional states and modes of nucleotide binding are indicated. **a**, $Ca_2E1{\sim}P$-AMPPN. **b**, E2-BeF_3^- structure with ADP (white stick) modelled at the N domain on the basis of the $Ca_2E1{\sim}P$-AMPPN structure. **c**, E2-$AlF4^-$-AMPPCP structure. **d**, E2-AMPPCP structure with thapsigargin (PDB 2C88). Functional state and mode of nucleotide binding are indicated on all panels.

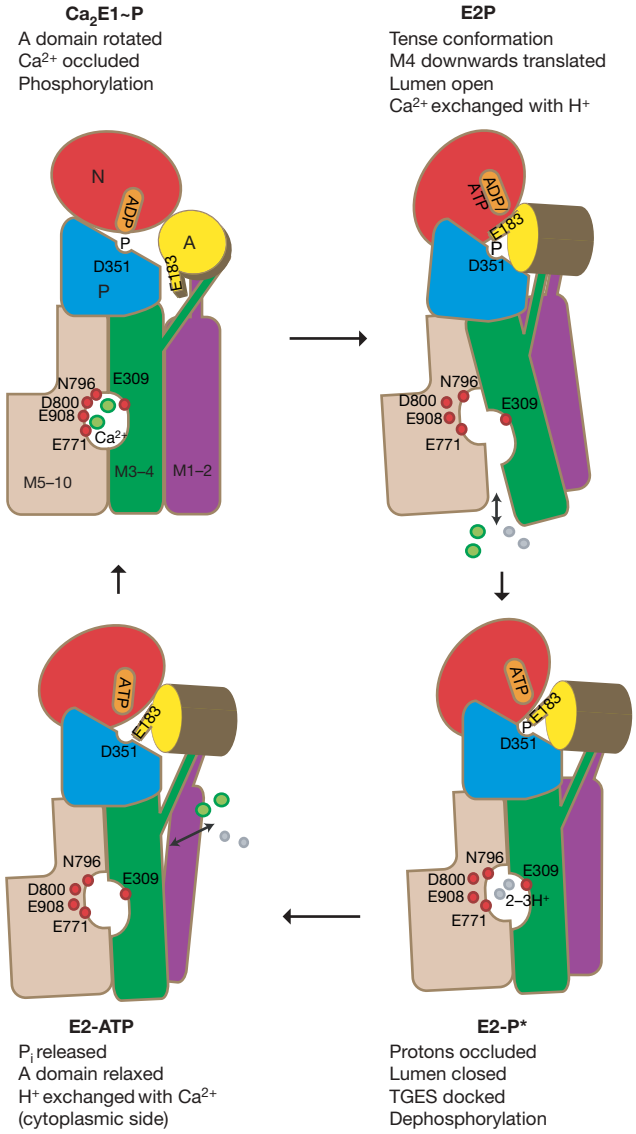

Figure 6 | Schematic representation of the reaction cycle. A schematic selection of key features of Ca^{2+}-ATPase function is indicated and reveals for the E2-P state the rotation of the A domain dragging M1–2, and the changes in the position of the P domain and N domain, pushing M3–4 in an outward and downward direction. See the Discussion for further detail. A domain, yellow; N domain, red; P domain, blue; helix M1–2, purple; M3–4, green; M5–10, wheat; Ca^{2+} ions and protons, green and grey spheres, respectively.

β,γ-phosphodiester bond breaks at the domain interface (Figs 2a and 5a). In the following step the A domain, with the conserved TGES loop, rotates towards the phosphorylation site, making firm associations with both the P domain and N domain. This movement exerts a downward push on the M3–M4 segment and a drag on the M1–M2 segment. In this transition, the configuration at the Ca^{2+}-binding residues in the membrane is forced apart, and the sites are favourably exposed to the polar environment of the luminal pathway to reduce the penalty of isolated charges in the membrane. During these movements, the cation-binding sites remain separated from the cytoplasm by a 15–20 Å thick barrier (Fig. 4b), whereas the N domain (left with ADP) is exposed to the cytosol and primed for ATP exchange (Fig. 5b), preventing a smooth reversal to the ADP-sensitive $Ca_2E1\sim P$ state.

Along with (partial) charge neutralization of the luminally exposed cation-binding sites by protons, a closure of the transmembrane segments becomes favourable, coupled to a downward rotation of the A domain and a movement of the P domain that leads the enzyme to the E2-P* transition state with occluded protons. In this state, the occluded protons are separated from the lumen by a 10–15 Å thick hydrophobic barrier (Fig. 4c) and a layer of positively charged residues at the luminal surface[14].

On dephosphorylation stimulated by the TGES motif, the cycle completes by release of the liberated phosphate stimulated by ATP binding[15] in the E2 state, with a cytoplasmic pathway opening for exchange of protons with calcium ions[10,15].

The pronounced conformational changes associated with Ca^{2+} translocation are in accordance with the role of Ca^{2+}-ATPase as a primary, active transporter. This is based on transitions between (at least) four different and well-defined conformational states, including the phosphoenzyme intermediates. A fundamental characteristic is a highly efficient separation between the cytoplasmic and extracellular/luminal environments at all steps in the cycle. The luminal pathway is broad and provides structural evidence for the long-sought E2P access channel on the basis of electrophysiological evidence[27,39] and from firmly anchored membrane transporters in general[40,41].

Glu 309 is a key player in Ca^{2+}-ATPase function, as previously pointed out[35,42] and can be described as a carrier of Ca^{2+} (and possibly protons) that moves up and down by about 6 Å with the M4 helix as the ATPase shuttles between E1 and E2 states (Fig. 6). Taken together, this pumping mechanism stands out as being powerful, and different to mechanisms based on narrow intramembranous pathways controlled by gating residues, such as those proposed for secondary transporters, like the lactose permease[43] and the sodium-coupled glutamate transporter[44]. At the same time, the coupled transport–counter-transport schemes are inherent to the system, compared to one-way transport of ABC transporters[45,46], and show a high resistance to backflow as compared to V-type ATPases; because of this, P-type ATPases perform well as electrogenic pumps.

The functional cycle of sarcoplasmic reticulum Ca^{2+}-ATPase rests on principles and structural elements that apply to all P-type ATPases. Indeed, P-type ATPases have been independently selected in fungi/plants (H^+-ATPase) and animals (Na^+,K^+-ATPase) for energization of strong plasma membrane potentials.

Finally, the open E2-BeF_3^- structure presented here provides a better template for modelling of the binding of clinically important inhibitors like omeprazole to H^+,K^+-ATPase (Supplementary Fig. 6), and ouabain to the Na^+,K^+-ATPase.

METHODS SUMMARY

Purification, crystallization and structure determination. Ca^{2+}-ATPase from rabbit fast-twitch skeletal muscle (SERCA1a) was prepared in sarcoplasmic reticulum membranes by differential centrifugations and solubilized by octaethyleneglycol dodecylether ($C_{12}E_8$) in buffers containing ligands as required for the formation of individual complexes. Supernatants from a final ultracentrifugation, with a protein concentration of approximately 12 mg ml^{-1}, were >90% pure and used directly for crystallization experiments. Crystals were obtained by the vapour diffusion method in hanging drops using PEG6000 or PEG2000 monomethyl-ether as the precipitant and *tert*-butanol, methylpentanediol (MPD), or dimethyl sulfoxide as additives.

Crystallographic data were collected at ESRF in Grenoble, France, and at EMBL/DESY in Hamburg (Supplementary Table 1). Structures were determined by molecular replacement (Supplementary Fig. 1) and the final model refinement employing the use of TLS parameterization was achieved with programs of the PHENIX package[47].

Detection of phosphorylated Ca^{2+}-ATPase by mass spectrometry. We developed a mass spectrometry method for detection of phosphorylation of Ca^{2+}-ATPase by AMPPNP, based on previous reports[48,49]. Fast hydrolysis of the aspartyl-phosphoanhydride residue prevents the direct detection by mass spectrometry. However, borohydrin reduction of the aspartyl-phosphoanhydride followed by CNBr treatment produces a Ca^{2+}-ATPase fragment (Met 327 to Met 361) with a stable homoserine occurring in place of phosphorylation at Asp 351. The peptide was identified and analysed by MALDI-TOF mass spectrometry (Supplementary Fig. 1).

Biochemical assays. The AMPPNP-supported Ca^{2+} transport by Ca^{2+}-ATPase-containing sarcoplasmic reticulum vesicles was assessed by current protocols[30,50] with particular care to avoid nucleotide contamination due to the low turn-over rate of AMPPNP-driven compared to ATP-driven transport (Supplementary Fig. 2). Ca^{2+} displacement of E2-BeF_3^- was followed by measuring the recovery of enzyme activity on Ca^{2+} addition; experiments using sarcoplasmic reticulum vesicles used the Ca^{2+} ionophore A23147 to differentiate between the effect of intravesicular and extravesicular Ca^{2+} (Supplementary Fig. 3).

Full Methods and any associated references are available in the online version of the paper at www.nature.com/nature.

Received 13 August; accepted 26 October 2007.

1. Rolfe, D. F. & Brown, G. C. Cellular energy utilization and molecular origin of standard metabolic rate in mammals. *Physiol. Rev.* **77,** 731–758 (1997).
2. Carafoli, E. Calcium signaling: a tale for all seasons. *Proc. Natl Acad. Sci. USA* **99,** 1115–1122 (2002).
3. Ebashi, S. & Lipmann, F. Adenosine triphosphate-linked concentration of calcium ions in a particulate fraction of rabbit muscle. *J. Cell Biol.* **14,** 389–400 (1962).
4. Hasselbach, W. Quantitative aspects of the calcium concept of excitation contraction coupling—a critical evaluation. *Basic Res. Cardiol.* **75,** 2–12 (1980).
5. De Meis, L. *The sarcoplasmic reticulum: Transport and Energy Transduction* (ed. Bittar, E. E.) (Wiley & Sons, New York, 1981).
6. Levy, D., Seigneuret, M., Bluzat, A. & Rigaud, J. L. Evidence for proton countertransport by the sarcoplasmic reticulum Ca^{2+}-ATPase during calcium transport in reconstituted proteoliposomes with low ionic permeability. *J. Biol. Chem.* **265,** 19524–19534 (1990).
7. Cornelius, F. & Moller, J. V. Electrogenic pump current of sarcoplasmic reticulum Ca^{2+}-ATPase reconstituted at high lipid/protein ratio. *FEBS Lett.* **284,** 46–50 (1991).
8. Yu, X., Carroll, S., Rigaud, J. L. & Inesi, G. H. + countertransport and electrogenicity of the sarcoplasmic reticulum Ca^{2+} pump in reconstituted proteoliposomes. *Biophys. J.* **64,** 1232–1242 (1993).
9. Toyoshima, C., Nakasako, M., Nomura, H. & Ogawa, H. Crystal structure of the calcium pump of sarcoplasmic reticulum at 2.6 Å resolution. *Nature* **405,** 647–655 (2000).
10. Toyoshima, C. & Nomura, H. Structural changes in the calcium pump accompanying the dissociation of calcium. *Nature* **418,** 605–611 (2002).
11. Sorensen, T. L., Moller, J. V. & Nissen, P. Phosphoryl transfer and calcium ion occlusion in the calcium pump. *Science* **304,** 1672–1675 (2004).
12. Toyoshima, C. & Mizutani, T. Crystal structure of the calcium pump with a bound ATP analogue. *Nature* **430,** 529–535 (2004).
13. Toyoshima, C., Nomura, H. & Tsuda, T. Lumenal gating mechanism revealed in calcium pump crystal structures with phosphate analogues. *Nature* **432,** 361–368 (2004).
14. Olesen, C., Sorensen, T. L., Nielsen, R. C., Moller, J. V. & Nissen, P. Dephosphorylation of the calcium pump coupled to counterion occlusion. *Science* **306,** 2251–2255 (2004).
15. Jensen, A. M., Sorensen, T. L., Olesen, C., Moller, J. V. & Nissen, P. Modulatory and catalytic modes of ATP binding by the calcium pump. *EMBO J.* **25,** 2305–2314 (2006).
16. Feher, J. J. & Briggs, F. N. Determinants of calcium loading at steady state in sarcoplasmic reticulum. *Biochim. Biophys. Acta* **727,** 389–402 (1983).
17. Gerdes, U. & Moller, J. V. The Ca^{2+} permeability of sarcoplasmic reticulum vesicles. II. Ca^{2+} efflux in the energized state of the calcium pump. *Biochim. Biophys. Acta* **734,** 191–200 (1983).
18. Yu, X. & Inesi, G. Variable stoichiometric efficiency of Ca^{2+} and Sr^{2+} transport by the sarcoplasmic reticulum ATPase. *J. Biol. Chem.* **270,** 4361–4367 (1995).
19. Artigas, P. & Gadsby, D. C. Na+/K+-pump ligands modulate gating of palytoxin-induced ion channels. *Proc. Natl Acad. Sci. USA* **100,** 501–505 (2003).

20. Tanford, C. Translocation pathway in the catalysis of active transport. *Proc. Natl Acad. Sci. USA* **80,** 3701–3705 (1983).
21. Toyoshima, C. & Inesi, G. Structural basis of ion pumping by Ca^{2+}-ATPase of the sarcoplasmic reticulum. *Annu. Rev. Biochem.* **73,** 269–292 (2004).
22. Takahashi, M., Kondou, Y. & Toyoshima, C. Interdomain communication in calcium pump as revealed in the crystal structures with transmembrane inhibitors. *Proc. Natl Acad. Sci. USA* **104,** 5800–5805 (2007).
23. Taylor, J. S. Sarcoplasmic reticulum ATPase catalyzes hydrolysis of adenyl-5′-yl imidodiphosphate. *J. Biol. Chem.* **256,** 9793–9795 (1981).
24. Meltzer, S. & Berman, M. C. Effects of pH, temperature, and calcium concentration on the stoichiometry of the calcium pump of sarcoplasmic reticulum. *J. Biol. Chem.* **259,** 4244–4253 (1984).
25. Mahaney, J. E., Thomas, D. D. & Froehlich, J. P. The time-dependent distribution of phosphorylated intermediates in native sarcoplasmic reticulum Ca^{2+}-ATPase from skeletal muscle is not compatible with a linear kinetic model. *Biochemistry* **43,** 4400–4416 (2004).
26. Skou, J. C. The Na,K-pump. *Methods Enzymol.* **156,** 1–25 (1988).
27. Läuger, P. in *Electrogenic pumps* Ch. 8 (Sinauer Associates, Sunderland, Massachusetts, 1991).
28. Danko, S., Yamasaki, K., Daiho, T. & Suzuki, H. Distinct natures of beryllium fluoride-bound, aluminum fluoride-bound, and magnesium fluoride-bound stable analogues of an ADP-insensitive phosphoenzyme intermediate of sarcoplasmic reticulum Ca^{2+}-ATPase: changes in catalytic and transport sites during phosphoenzyme hydrolysis. *J. Biol. Chem.* **279,** 14991–14998 (2004).
29. Picard, M., Toyoshima, C. & Champeil, P. Effects of inhibitors on luminal opening of Ca^{2+} binding sites in an E2P-like complex of the sarcoplasmic reticulum Ca^{2+}-ATPase with Be^{2+}-fluoride. *J. Biol. Chem.* **281,** 3360–3369 (2006).
30. Moller, J. V. *et al.* Calcium transport by sarcoplasmic reticulum Ca^{2+}-ATPase. Role of the A domain and its C-terminal link with the transmembrane region. *J. Biol. Chem.* **277,** 38647–38659 (2002).
31. Daiho, T. *et al.* Deletions of any single residues in Glu^{40}–Ser^{48} loop connecting a domain and the first transmembrane helix of sarcoplasmic reticulum Ca^{2+}-ATPase result in almost complete inhibition of conformational transition and hydrolysis of phosphoenzyme intermediate. *J. Biol. Chem.* **278,** 39197–39204 (2003).
32. Lenoir, G. *et al.* Functional properties of sarcoplasmic reticulum Ca^{2+}-ATPase after proteolytic cleavage at Leu^{119}–Lys^{120}, close to the A-domain. *J. Biol. Chem.* **279,** 9156–9166 (2004).
33. Daiho, T., Yamasaki, K., Danko, S. & Suzuki, H. Critical role of Glu^{40}–Ser^{48} loop linking actuator domain and 1st transmembrane helix of Ca2+-ATPase in Ca2+ deocclusion and release from ADP-insensitive phosphoenzyme. *J. Biol. Chem.* **282,** 34429–34447 (2007).
34. Andersen, J. P. & Vilsen, B. Structure–function relationships of cation translocation by Ca^{2+}- and Na+, K+-ATPases studied by site-directed mutagenesis. *FEBS Lett.* **359,** 101–106 (1995).
35. Vilsen, B. & Andersen, J. P. Mutation to the glutamate in the fourth membrane segment of Na+,K+-ATPase and Ca^{2+}-ATPase affects cation binding from both sides of the membrane and destabilizes the occluded enzyme forms. *Biochemistry* **37,** 10961–10971 (1998).
36. Morth, J. P. *et al.* Crystal structure of the sodium–potassium pump. *Nature* doi:10.1038/nature06419 (this issue).
37. Reyes, N. & Gadsby, D. C. Ion permeation through the Na+,K+-ATPase. *Nature* **443,** 470–474 (2006).
38. Wakabayashi, S., Ogurusu, T. & Shigekawa, M. Factors influencing calcium release from the ADP-sensitive phosphoenzyme intermediate of the sarcoplasmic reticulum ATPase. *J. Biol. Chem.* **261,** 9762–9769 (1986).
39. Apell, H. J. Structure–function relationship in P-type ATPases–a biophysical approach. *Rev. Physiol. Biochem. Pharmacol.* **150,** 1–35 (2003).
40. Jardetzky, O. Simple allosteric model for membrane pumps. *Nature* **211,** 969–970 (1966).
41. Vidaver, G. A. Inhibition of parallel flux and augmentation of counter flux shown by transport models not involving a mobile carrier. *J. Theor. Biol.* **10,** 301–306 (1966).
42. Inesi, G., Ma, H., Lewis, D. & Xu, C. Ca^{2+} occlusion and gating function of Glu^{309} in the ADP-fluoroaluminate analog of the Ca^{2+}-ATPase phosphoenzyme intermediate. *J. Biol. Chem.* **279,** 31629–31637 (2004).
43. Abramson, J. *et al.* Structure and mechanism of the lactose permease of *Escherichia coli*. *Science* **301,** 610–615 (2003).
44. Boudker, O., Ryan, R. M., Yernool, D., Shimamoto, K. & Gouaux, E. Coupling substrate and ion binding to extracellular gate of a sodium-dependent aspartate transporter. *Nature* **445,** 387–393 (2007).
45. Dawson, R. J. & Locher, K. P. Structure of a bacterial multidrug ABC transporter. *Nature* **443,** 180–185 (2006).
46. Hvorup, R. N. *et al.* Asymmetry in the structure of the ABC transporter–binding protein complex BtuCD–BtuF. *Science* **317,** 1387–1390 (2006).
47. Adams, P. D. *et al.* PHENIX: building new software for automated crystallographic structure determination. *Acta Crystallogr. D* **58,** 1948–1954 (2002).
48. Collet, J. F., Stroobant, V. & Van Schaftingen, E. Evidence for phosphotransferases phosphorylated on aspartate residue in N-terminal DXDX(T/V) motif. *Methods Enzymol.* **354,** 177–188 (2002).
49. Purich, D. L. Use of sodium borohydride to detect acyl-phosphate linkages in enzyme reactions. *Methods Enzymol.* **354,** 168–177 (2002).
50. Fiske, C. H. & Subbarow, Y. The colorimetric determination of phosphours. *J. Biol. Chem.* **26,** 375–400 (1925).

Supplementary Information is linked to the online version of the paper at www.nature.com/nature.

Acknowledgements We dedicate this paper to the memory of B. Holm. We thank B. Nielsen, M.-B. Hemmingsen and A. M. Nielsen for technical assistance; J. L. Karlsen and F. Fredslund for technical discussions; and D. Flot and L. Gordon at beamlines ID 23-1 and -2 (operated jointly with EMBL-Grenoble) and ID 29 at the European Synchrotron Radiation Facility (ESRF) for help with data collection. Beamtime at the EMBL-DESY synchrotron Hamburg Germany is also acknowledged. This work was supported by the Danish Natural Science Research Council through the DANSYNC program, the Danish Medical Research Council, the Aarhus University Research Foundation, and the Novo Nordisk Foundation. C.Ol. is the recipient of a stipend from the PC Petersen Foundation and a PhD fellowship from the faculty of Health Sciences Aarhus University. A PhD fellowship (A.-M.L.W.) was financed by the Lundbeck Foundation. M.P. was supported by a post-doctoral fellowship from the Federation of European Biochemical Societies (FEBS) and P.N. is supported by a Hallas-Møller stipend of the Novo Nordisk Foundation.

Author Contributions C.Ol., M.P., A.-M.L.W., J.V.M. and P.N. contributed equally to this work. J.P.M. assisted with data collection and structure determination. C.Ox. and C.G. contributed with mass-spectrometry data and analysis.

Author Information The structural data have been deposited with the following codes in the Protein Data Bank: Ca2E1~P, 3BA6; E2-AlF4$^-$, 3B9R; and E2-BeF3$^-$, 3B9B. Reprints and permissions information is available at www.nature.com/reprints. Correspondence and requests for materials should be addressed to P.N. (pn@mb.au.dk) and J.V.M. (jvm@biophys.au.dk).

METHODS

Purification and solubilization. Ca^{2+}-ATPase prepared from rabbit fast twitch skeletal muscle (SERCA1a) was purified from sarcoplasmic reticulum vesicles according to established procedures[51].

$Ca_2E1\sim P$ crystals were obtained by solubilization with 30 mM octaethyleneglycol dodecylether ($C_{12}E_8$) in 100 mM MOPS-KOH, pH 6.8, 20% (w/v) glycerol, 80 mM KCl, 5 mM AMPPNP and 10 mM $CaCl_2$. The E2-BeF_3^- crystals were obtained by solubilization with 30 mM $C_{12}E_8$ in 100 mM MOPS-KOH, pH 7.0, 50 mM LiCl, 5 mM $MgCl_2$, 2 mM EGTA, 5 mM NaF and 0.66 mM $BeSO_4$. The E2-AlF_4^--AMPPCP complex was solubilized with 35 mM ($C_{12}E_8$) in 100 mM MOPS-KOH, pH 6.8, 20% glycerol, 80 mM KCl, 3 mM $MgCl_2$, 2 mM EGTA and 1 mM AMPPCP.

Crystallization. The solubilization was followed by ultracentrifugation at 4 °C for 35 min at 50,000 r.p.m. in a Beckman TLA-110 rotor. The protein was stored on ice overnight and then subjected again to ultracentrifugation for 15 min at 70,000 r.p.m. Supernatants, with a protein concentration of approximately 12 mg ml^{-1}, were > 95% pure and used directly for crystallization experiments. The hanging drop method was applied (at 19 °C) by mixing 2 µl of protein solution with 2 µl of crystallization buffer solution composed in the following way: $Ca_2E1\sim P$, 8% (w/v) PEG6000, 15% (w/v) glycerol, 200 mM sodium acetate, 4% (v/v) tert-butanol and 5 mM β-mercaptoethanol; E2-BeF_3^-, 18% (w/v) PEG 6000, 50 mM $MgSO_4$, 10% (v/v) glycerol and 4% DMSO; E2-AlF^--AMPPCP, 12% (w/v) PEG2000 mono-methylether, 200 mM $MgSO_4$ and 6% MPD.

Large, single crystals grew within a week for the $Ca_2E1\sim P$-AMPPN form and 2–3 weeks for the E2-BeF_3^- and E2-AlF_4^- forms. Crystals were taken directly from the mother liquor after limited dehydration ($Ca_2E1\sim P$-AMPPN) or on addition of glycerol to crystallization drops for cryo-protection (E2-BeF_3^- and E2-AlF_4^- crystals), mounted in nylon loops, and flash-cooled in liquid nitrogen, as described[52].

Data collection. Crystallographic data were collected at the beamlines ID23-2 and ID29 ESRF (European Synchrotron Radiation Facility) Grenoble, France, and EMBL/DESY (The EMBL X11 beamline at the DORIS storage ring, DESY) Hamburg, Germany. Data processing was performed with XDS[53], and phases obtained by molecular replacement using partial search models and the PHASER program[54]. The initial molecular replacement phases were refined by density modification through the RESOLVE prime-and-switch routine[55] (Supplementary Fig. 4) and later stages of model building were carried out on the basis of omit maps and $2F_O-F_C$ maps using O[56]. Refinement of structures was performed with the CNS program[57]. Final model refinement employing the use of TLS parameterization was achieved with programs of the PHENIX package[47]. The structures were validated using PROCHECK[58].

MALDI-TOF analysis of phosphoenzyme and crystal samples. Direct detection of the aspartyl-phosphoanhydride residue by mass spectrometry is not possible owing to nearly instant hydrolysis[59]. Instead we have used $NaBH_4$ to specifically reduce the aspartyl-phosphoanhydride into a stable homoserine residue[48,49,60–62]. Control samples of SERCA1a phosphoenzyme were made by incubating, on ice, sarcoplasmic reticulum vesicles at 0.2 mg of protein per ml in 50 mM MOPS (3-(*N*-morpholino)propanesulfonic acid) titrated with Tris (2-amino-2-hydroxymethyl-1,3-propanediol) at pH 7.8, 100 mM KCl, 5 mM $MgCl_2$, 50 µM $CaCl_2$ in the presence or in the absence of 5 µM ATP. The reactions were quenched by adding ice-cold 10% (w/v) trichloroacetic acid (TCA 10%) after 20 s of reaction. All samples were then kept on ice for 20 min and centrifuged for 20 min at 4,300 r.p.m. in a bench-top centrifuge (4 °C). Pellets were resuspended in 750 µl of ice-cold 5% TCA and centrifuged for 10 min at 72,000 r.p.m. in a Beckman TLA-110 rotor (at 4 °C). The pellets were finally rinsed in 10 mM ice-cold HCl, centrifuged 5 min at 72,000 r.p.m. and lyophilized.

Reduction of the aspartyl-phosphoanhydride to homoserine was performed by adding 100 µl of freshly prepared 10 µM $NaBH_4$ solution, suspended in 100 µl of DMSO, to the pellets. Incubation was performed for 20 min and quenched by addition of 200 µl of ice-cold 0.44 M $KClO_4$. After 30 min incubation on ice, the samples were centrifuged at 50,000 r.p.m. for 20 min in a Beckman TLA-110 rotor and the pellets lyophilized.

Crystals of the $Ca_2E1\sim P$-AMPPN form were harvested with crystal mounting loops and transferred to ice-cold TCA 10% with further manipulations, including $NaBH_4$ reduction, as described above.

Cyanogen Bromide (CNBr) fragmentation was performed by incubating the $NaBH_4$-reduced material with a 100-fold molar excess of CNBr over methionine. CNBr was dissolved in 70% trifluoroaceticacid (TFA) and the reactions were incubated overnight at room temperature. The patterns of fragmentation were compared for the different samples by matrix-assisted laser desorption ionization time-of-flight (MALDI-TOF) mass spectrometry (Supplementary Fig. 1). Mass spectra were acquired with a Voyager-DE PRO (MALDI-TOF) instrument (Applied Biosystems) operated in linear mode. Samples were prepared by crystallization of the peptide analytes with α-cyano-4-hydroxycinnamic acid. Final spectra were obtained by averaging 200 single shot spectra, and calibrated externally

AMPPNP-supported Ca^{2+} uptake by sarcoplasmic reticulum vesicles. Active Ca^{2+} transport by sarcoplasmic reticulum vesicles was measured by Millipore filtration with the aid of $^{45}Ca^{2+}$, according to current protocols but with the inclusion of some precautions arising from the slow rates of uptake sustained by the ATP analogue. The sarcoplasmic reticulum vesicles were kept suspended at a protein concentration of 0.2–1 mg ml^{-1} in a 30 mM imidazole buffer, pH 7.1, containing 150 mM NaCl, 5 mM Mg^{2+}, 0.10 mM $^{45}Ca^{2+}$ in the presence of various concentrations of AMPPNP (5–800 µM). Aliquots (comprising 200 µg of protein) were quenched at different time periods with 4 ml of unlabelled and ice-cold buffer, without added Ca^{2+}, and the vesicles were deposited on a 0.45 µm Millipore filter and further rinsed twice with 3 ml of ice-cold buffer. We found that when Ca^{2+} uptake measurements were performed in this way, there was a slow, time-dependent rise in Ca^{2+} retained by the filter, preceded by a jump in Ca^{2+} accumulation, occurring immediately after the addition of AMPPNP (Supplementary Fig. 2). This jump (the presence of which is also apparent from a previous report[23]) is not attributable to inefficient removal of Ca^{2+} bound on the outside of the vesicles, which shows that only small amounts of Ca^{2+} are retained on the filter in the absence of AMPPNP. Instead it is probably caused by rapid hydrolysis of ATP contaminating the AMPPNP reagent. In agreement with this view we found that the extent of the jump (which at a concentration of 0.8 mM nucleotide would correspond to a contamination of the order of 1.25–2.5%, assuming a coupling ratio between 1 and 2) was proportional to the concentration of AMPPNP. To remove contaminating ATP we routinely started the Ca^{2+} uptake experiments by pre-incubating the AMPPNP and $^{45}Ca^{2+}$ containing incubation medium with purified and leaky Ca^{2+}-ATPase membranes (at 0.050 mg of protein per ml) for 15 min, before starting the Ca^{2+} uptake experiments by the addition of sarcoplasmic reticulum vesicles. This protocol results in a regular uptake curve that eventually (after 90 min) leads to the same accumulation as observed without the pre-treatment with the leaky Ca^{2+}-ATPase membranes (Supplementary Fig. 2). From such curves, we could calculate the initial rates of Ca^{2+} transport after subtraction of a minor contribution (corresponding to 2–4 nmol of Ca^{2+} per mg of protein) that was measured immediately after the sarcoplasmic reticulum addition both in the presence and absence of AMPPNP and thus not attributable to Ca^{2+} transport.

Reaction of Ca^{2+}-ATPase with beryllium fluoride and Ca^{2+} reactivation. The use of beryllium fluoride (BeF_3^-) as a structural analogue of phosphorylation that forms an inhibitory complex with SERCA1a was pioneered by Murphy and Coll[63]. Intrinsic fluorescence and other evidence showing that complexation is compatible with the formation of an E2P state with luminally oriented Ca^{2+}-binding sites were later provided[28,29]. In our experiments, we find that in Ca^{2+}-depleted EGTA media Ca^{2+}-ATPase reacts with BeF_3^- by an irreversible reaction, characterized by apparent rate constants of 22 mM^{-1} min^{-1} at pH 7.2 and 13 mM^{-1} min^{-1} at pH 6.0, and eventually leading to complete inhibition of enzyme activity by low (micromolar) concentrations of BeF_3^-, provided that BeF_3^- is present in larger than stoichiometric amounts compared to SERCA1a (Supplementary Fig. 3). However, the stability of the complex is more sensitive to the presence of Ca^{2+} (Fig. 3) as compared to the E2-AlF_4^- complex[14,28]. This creates the problem when using enzymatic spectrophotometry[64] to follow BeF_3^- on- and off-reactions that unwanted re-activation readily occurs during the assay, resulting in downward deflecting curves (Supplementary Fig. 3). To minimize assay-induced re-activation we performed these measurements at low Ca^{2+} concentrations (at [Ca^{2+}]/[EGTA] concentration ratios of 0.9:1) and low ATP concentrations (0.1 mM instead of 5 mM MgATP), which resulted in nearly linear traces.

51. Andersen, J. P., Lassen, K. & Moller, J. V. Changes in Ca^{2+} affinity related to conformational transitions in the phosphorylated state of soluble monomeric Ca^{2+}-ATPase from sarcoplasmic reticulum. *J. Biol. Chem.* **260**, 371–380 (1985).
52. Sorensen, T. L., Olesen, C., Jensen, A. M., Moller, J. V. & Nissen, P. Crystals of sarcoplasmic reticulum Ca^{2+}-ATPase. *J. Biotechnol.* **124**, 704–716 (2006).
53. Kabsch, W. Automatic processing of rotation diffraction data from crystals of initially unknown symmetry and cell constants. *J. Appl. Cryst.* **26**, 795–800 (1993).
54. McCoy, A. J., Grosse-Kunstleve, R. W., Storoni, L. C. & Read, R. J. Likelihood-enhanced fast translation functions. *Acta Crystallogr. D* **61**, 458–464 (2005).
55. Terwilliger, T. C. Maximum-likelihood density modification. *Acta Crystallogr. D* **56**, 965–972 (2000).
56. Jones, T. A., Zou, J. Y., Cowan, S. W. & Kjeldgaard, M. Improved methods for building protein models in electron density maps and the location of errors in these models. *Acta Crystallogr. A* **47**, 110–119 (1991).

57. Brunger, A. T. *et al.* Crystallography & NMR system: A new software suite for macromolecular structure determination. *Acta Crystallogr. D* **54,** 905–921 (1998).
58. Laskowski, R. A., Moss, D. S. & Thornton, J. M. Main-chain bond lengths and bond angles in protein structures. *J. Mol. Biol.* **231,** 1049–1067 (1993).
59. Sickmann, A. & Meyer, H. E. Phosphoamino acid analysis. *Proteomics* **1,** 200–206 (2001).
60. Allegrini, S. *et al.* Bovine cytosolic 5′-nucleotidase acts through the formation of an aspartate 52-phosphoenzyme intermediate. *J. Biol. Chem.* **276,** 33526–33532 (2001).
61. Collet, J. F., Stroobant, V. & Van Schaftingen, E. Mechanistic studies of phosphoserine phosphatase, an enzyme related to P-type ATPases. *J. Biol. Chem.* **274,** 33985–33990 (1999).
62. Sanders, D. A., Gillece-Castro, B. L., Stock, A. M., Burlingame, A. L. & Koshland, D. E. Jr. Identification of the site of phosphorylation of the chemotaxis response regulator protein, CheY. *J. Biol. Chem.* **264,** 21770–21778 (1989).
63. Murphy, A. J. & Coll, R. J. Fluoride is a slow, tight-binding inhibitor of the calcium ATPase of sarcoplasmic reticulum. *J. Biol. Chem.* **267,** 5229–5235 (1992).
64. Moller, J. V., Lind, K. E. & Andersen, J. P. Enzyme kinetics and substrate stabilization of detergent-solubilized and membraneous (Ca^{2+} + Mg^{2+})-activated ATPase from sarcoplasmic reticulum. Effect of protein–protein interactions. *J. Biol. Chem.* **255,** 1912–1920 (1980).